Band structure and x-ray photoelectron spectrum of ZrB$_2$

Hideo Ihara, Masayuki Hirabayashi, and Hiroshi Nakagawa

Electrotechnical Laboratory, Tanashi, Tokyo

The band structure and the density of states of ZrB$_2$ have been calculated by an augmented-plane-wave method and compared with the observed x-ray photoelectron spectrum of valence band. The theoretical energy-distribution curve obtained by using the Kohn-Sham exchange potential was in good agreement with the experimental one. The calculated density of states at the Fermi level and the interband transition energies at the Γ point were consistent with the available experimental data of a low-temperature specific heat and a reflectance measurement. The band structure shows that the bonding nature of ZrB$_2$ can be explained by a combination of the graphitic bonding model of boron network and the hcp-metal bonding model of zirconium.

I. INTRODUCTION

Transition-metal borides have several unique properties among which are high melting point, hardness, chemical stability, and metallic property as seen in transition-metal carbides. For the lack of convincing evidences for their band structures, many conflicting theories about their bonds and electronic structures have been proposed to explain those properties.[1-6] These theories can be attributed to two distinct bonding models for transition-metal diborides with a hexagonal lattice of AlB$_2$ type.[7] One is the graphitic bonding model of planar layers of boron hexagon.[1-3] The other is the interstitial compound model.[4-6]

The former model indicates that the metal atom forms a positive bivalent ion and that the negative boron ion framework is isoelectronic with that of graphite.[1] This model is used to explain the NMR data within the framework of metal-boron donor-acceptor bonds on the assumption of a $(sp^2)p_z$ configuration of the boron atom.[2] A modified linear-combination-of-atomic-orbitals calculation leads to the fact that the statistical weights of the contribution of the boron sp^2 configuration are larger than those of the metal atom's d^5 configuration.[3] This model is good for explaining the charge transfer from metal to boron, the existence of covalent bond, hardness, brittleness, and high melting point.

The latter model indicates that the band structure of the transition metal remains approximately the same as boron enters the metal lattice and the boron atoms donate electrons to the d band of the metal. On the basis of this model Dempsey has systematically interpreted melting points and electrical resistivities of transition-metal compounds in terms of assumed d-electron numbers.[4] The low-temperature specific-heat data have been interpreted as if the band structures of the borides closely resemble those of the pure-transition-

metal elements and the Fermi level lies in a broad conduction band separating the bonding and anti-bonding parts.[5] The Hall effect has been explained to suggest that the d bands are completely filled by the contribution of three electrons from each boron atom and the main conduction band is an s band.[6] This model is good for explaining the charge transfer from boron to metal, metallic properties, and high melting points.

The calculated band structures of CrB$_2$ and TiB$_2$ are not fully consistent with each other nor with the above-mentioned models. Both band calculations of CrB$_2$ from the augmented plane wave (APW) method[8] and the Korringa-Kohn-Rostoker (KKR) method[9] predict the reverse directions in charge transfer between boron and metal. The band structure of CrB$_2$ from the KKR method can explain fairly well the electronic specific-heat of a series of diboride compounds by using a rigid-band model. This approach, however, gives a disagreement with the result of TiB$_2$ tight-binding calculation in which a part of the graphitic band structure and the charge transfer from titanium to boron are present.[10]

Therefore it is necessary to study the band structures of diborides in greater detail from both experimental and theoretical sides. One of the most promising techniques for investigation of the band structure of a metallic compound would be the interplay between the APW calculation and the x-ray photoelectron spectroscopy (XPS). That is demonstrated in the case of transition-metal carbides.[11,12]

In this paper the XPS spectrum of valence band of ZrB$_2$ is observed and the band structures and the densities of states (DOSs) are calculated by the APW method altering the crystal potential. The theoretical energy distribution curves (EDCs) from the DOSs are compared with the XPS-EDC. The resulting band structures are discussed in comparison with such available experimental data as

the interband transition energies from optical reflectance,[13] and electronic specific-heat,[5] and x-ray emission spectra of TiB_2.[14,15]

II. EXPERIMENT AND RESULTS

Zirconium diborides samples were prepared by both the arc-melting and the hot-pressing techniques.[16] (a) The mixtures of zirconium and boron powders were arc-melted in an argon atmosphere. Then it was annealed at a temperature of 2000 °C for 2 h to improve the homogeneity. The sample contained no extra phase except ZrB_2. (b) The powders of ZrB_2 were hot-pressed in a graphite die at 2200 °C and 300 kg/cm² in an atmosphere of 5×10^{-4} Torr for 30 min. The core of the hot-pressed sample was used to avoid carbon impurity from the die.

After polishing with diamond paste the specimen of ZrB_2 was heated at around 1600 °C in a pressure of 1×10^{-8} Torr for 5 h to eliminate the surface contaminants such as carbides and oxides. Then the sample was inserted into the XPS analyzing chamber without exposing to the air. The measurement was performed on an HP 5950A ESCA spectrometer with a resolution of 0.6 eV. The spectra from both specimens prepared by different techniques, arc-melting and hot-pressing, showed no particular contrast. The contamination of carbon was eliminated, but oxygen could not be eliminated completely by the sample treatment. The core-level peaks of zirconium dioxide were observed even when great care was exercised, though boron oxide was not detected. The extent of contribution of zirconium dioxide to the valence band can be estimated from the XPS spectrum itself, since the integrated intensities of Zr $4d$ lines represent the amounts of the zirconium diboride and the zirconium dioxide. Then the contribution of oxide to the valence-band spectrum was compensated by the data treatment.

Figure 1 shows the experimental EDC obtained by subtracting the contribution of oxide and a background due to inelastically scattered electrons from the observed XPS spectrum. The charac-
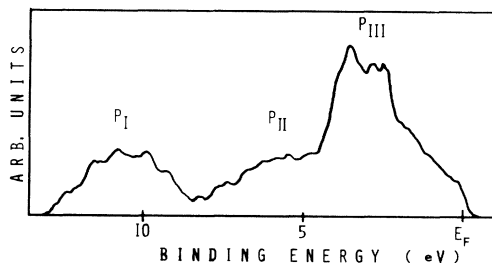
teristic features of the EDC are divided into three parts of P_I, P_{II}, and P_{III} which lies with the almost same energy width as shown in Fig. 1. The peaks of P_{III}, P_{II}, and P_I are ranging from the Fermi level to 4.5, from 4.5 to 8.5 and from 8.5 to 13 eV, respectively. The peaks P_{III} and P_I are located at 3.2 and 10.4 eV.

III. BAND CALCULATION

Band calculation was performed by the APW method using the Slater exchange potential or the Kohn-Sham (KS) one[17] and considering a sufficient number of neighbor atoms up to the 14th neighbors by means of the Lowdin α expansion.[18] The potentials of the constituent atoms were calculated by assuming the neutral atomic configurations of $B(2s)^2(2p)^1$ and $Zr(4d)^2(5s)^2$ with the program of Herman and Skillman.[19] The computational procedure used in this work is similar to that described by Loucks.[20] The radius of muffin-tin potential (MTP) of boron was chosen to be close to one half of the B–B bond length and the zirconium MTP radius was determined to be less than the difference between the Zr–B bond length and the boron MTP radius. The relevant potential parameters are listed in Table I. The energy values were calculated on a grid of 160 points in $\frac{1}{24}$ of the Brillouin zone. The convergence of eigenvalues below the Fermi level was within 0.01 Ry around Γ point and within 0.02 Ry around the boundary of the Brilloiun zone with 35 reciprocal-lattice vectors. The vectors which are determined from the convergence study in the wave function expansion are listed in Table II.

The band structure and the DOS of ZrB_2 obtained by using the KS exchange potential are shown in Fig. 2. The valence-band DOS consists of three characteristic peaks marked with P_I, P_{II}, and P_{III}. The peak P_I corresponds to the first band (numbering the bands in ascending order of energy) arising from the B $2s$ state. The broad peak range P_{II} is related to bands 2 and 3 which are attributed

FIG. 1. X-ray photoelectron spectrum of ZrB_2.

TABLE I. Lattice constant, APW sphere radius, and constant part of the potential used in the band calculation of ZrB_2 in atomic units (1 a.u. = 0.5292 Å, 1 Ry = 13.605 eV).

Lattice constant (a.u.)	R_s (a.u.)	V_c (Ry)
a: 5.989	B: 1.649	−1.267; Kohn–Sham exchange
c: 6.671	Zr: 2.586	−1.548; Slater exchange

TABLE II. 35 reciprocal lattice vectors used in the present calculation.

Vector				Vector			
1	0	0	0	21	−1	1	0
2	−1	0	0	22	0	1	−1
3	1	0	0	23	−2	0	−1
4	0	−1	0	24	−1	1	−1
5	0	−1	1	25	−2	0	1
6	−1	−1	0	26	2	−1	0
7	−1	−1	1	27	2	0	−1
8	0	0	−1	28	1	1	−1
9	1	−1	0	29	2	−1	1
10	−1	0	−1	30	1	1	0
11	−2	0	0	31	0	−1	−1
12	1	−1	1	32	0	−2	1
13	−2	−1	0	33	−1	−1	−1
14	−2	−1	1	34	−1	−2	1
15	0	0	1	35	−3	0	0
16	−1	0	1				
17	1	0	−1				
18	2	0	0				
19	1	0	1				
20	0	1	0				

to the B $2p$ state. The peak P_{III} corresponds to bands 3 to 5. The flat parts of bands 4 and 5 are associated with the top of this peak which is derived from the Zr $4d$ state. The Fermi level is located at the vicinity of the minimum point of the DOS. The DOS at that point is 0.22 electrons/ (eV primitive cell).

Figure 3 shows the band structure and the DOS obtained by using the full Slater exchange potential. The band structure has similar features to that of Fig. 2, but the valence-band width is narrower than that of Fig. 2 by 2.1 eV. The DOS at the Fermi level is 0.30 electrons/(eV primitive cell).

IV. DISCUSSION

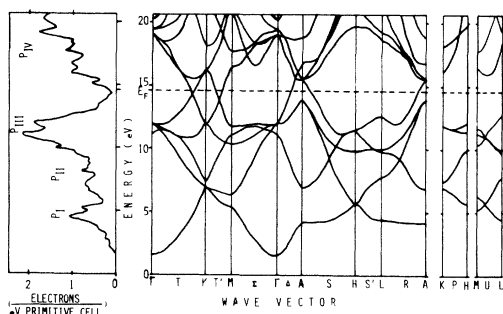The theoretical EDCs were derived from the calculated DOSs by assuming a Gaussian smearing
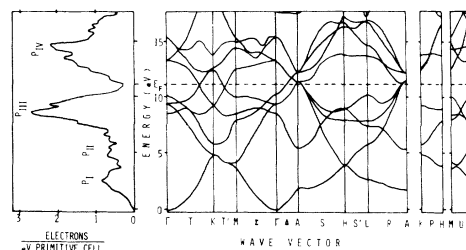

FIG. 3. Density of states and the band structure of ZrB_2 calculated using the full Slater exchange potential.

function with the full width at half maximum of 0.6 eV. The Gaussian function is more suitable as the smearing function near the Fermi level of ZrB_2 than the Lorentzian. Figure 4 shows the comparison between the theoretical EDC obtained by using the KS exchange potential (solid line) and the experimental EDC (dashed line). The characteristic features of the theoretical EDC can be related to the corresponding features of the experimental one. The agreement is particularly good in the outline of the EDC, the width of valence band and the energies of three peaks. The binding energies of peak P_{III} coincide within 0.2 eV.

On the other hand, the difference between those EDCs is observed around the Fermi level. The intensity of the experimental spectrum at that point is enhanced in contrast with the theoretical EDC. This enhancement is probably owing to the cross-section modulation of d electron. Such phenomenon has been observed in the XPS spectra of transition-metal carbides.[12]

The other theoretical EDC (solid line) obtained by using the full Slater exchange potential is compared with the experimental one in Fig. 5. The resemblance between them is not better than in Fig. 4. Although the outlines of those EDCs resemble a little the theoretical width of valence band is narrower than the experimental one by 2 eV. The characteristic features of the experimental EDC and both the theoretical EDCs are compared in

FIG. 2. Density of states and the band structure of ZrB_2 calculated using the Kohn-Sham exchange potential.
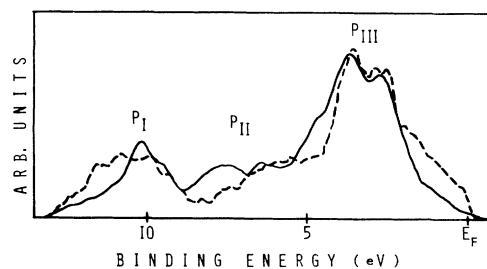

BINDING ENERGY (eV)

FIG. 4. Comparison between the theoretical energy distribution curve (EDC) from the Kohn-Sham exchange potential (solid line) and the experimental EDC (dashed line).
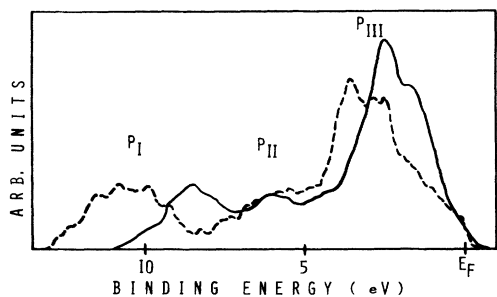
FIG. 5. Theoretical EDC from the Slater exchange potential (solid line) compared with the experimental EDC (dashed line).

Table III. The KS exchange potential gives a better agreement of the theoretical EDC with the XPS-EDC than the Slater exchange potential. This result contrasts with the transition-metal carbides in which the Slater exchange potential is good.[11,12]

The comparison of the XPS-EDC with the DOS of CrB_2 suggests that the rigid-band model is not a good approximation in order to derive the DOS of ZrB_2 from that of CrB_2 which is calculated with the Slater exchange potential.[9] The differences between them are remarkable in the valence-band width and the binding energy and features of peak P_{III}. Although both the present calculated band structure of ZrB_2 are apparently shaped like that of CrB_2 in the valence-band region, the widths of valence band of ZrB_2 are narrower than that corresponding to TiB_2 obtained from the CrB_2 band structure assuming the rigid-band model. The difference between their bandwidths is 4.1 eV in the case of using the Slater exchange potential.

The interband transitions of 6.75 and 7.75 eV have been indicated from the reflectance measurement.[13] The band structure obtained by using the KS exchange potential shows the existence of interband transition of 6.7 and 7.9 eV around the Γ point. The former transition occurs between three degenerate bands 3 to 5 and three nearly degenerate bands 6 to 8. The latter occurs between three bands 3 to 5 and two degenerate bands 11 and 12. Other transitions are possible, but their intensi-

ties would be weak because of small DOSs of related bands.

The low-temperature specific heat has given the DOS at the Fermi level of 0.20 electrons/(eV primitive cell).[5] This value is close to 0.22 from the theoretical DOS with the KS exchange potential, but smaller than 0.30 from the Slater exchange potential. The electronic specific-heat data has been explained on the basis of the interstitial compound model. Then Tyan *et al.* speculate a band model in which the Fermi level lies in a broad conduction band separating the bonding and antibonding parts.[5] The present band structure supports that band model.

The Ti $L_{II, III}$-x-ray emission spectrum of TiB_2 shows the presence of a peak with two heads at 1.7 and 3.1 eV and a hump at 6.7 eV below the Fermi level.[14] The outline of that spectrum resembles the part of P_{III} and P_{II} of the theoretical EDC of ZrB_2 in spite of disagreement in binding energy. On the other hand, Ti K-emission spectrum of TiB_2 shows a broad single peak at 3.7 eV and a hump at 11 eV.[15] That spectrum has a shape obtained by smearing the theoretical DOS of ZrB_2.

In comparison of the XPS-EDC with the DOS of graphite[21,22] and the DOS of zirconium metal,[23] several resemblances are observed. The features of peak P_{III} are shaped like those of the zirconium DOS, though the position of the peak P_{III} is lowered by 2.0 eV. The shape of a range of peaks P_I and P_{II} resembles the valence-band XPS spectrum of graphite, though the total width of ZrB_2 valence band is narrower than that of graphite by a factor of 2. The XPS-EDC implies that the band structure of ZrB_2 is like a hybrid structure of those of graphite and zirconium metal.

The calculated DOS of valence band of ZrB_2 has a shape composed of both the zirconium DOS[23] and the graphite DOS[21,22] in disregard of the difference in the band width. Bands 1, 2, 3, and 5 in the ZrB_2 band structure show the behavior like the graphitic band structure along the $\Gamma KM\Gamma$ symmetry line.[17] This leads to the fact that bands 1, 2, and 3 correspond to the sp^2 hybrid state and band 5 has π or p_z character on the analogy of the structure.

TABLE III. Comparison of the theoretical EDCs with the experimental EDC.

	Full width of valence band (eV)	Binding energy (eV)		Full width at half maximum (eV)		DOS at the Fermi level $\left(\dfrac{\text{electrons}}{\text{eV primitive cell}}\right)$
		P_I	P_{III}	P_I	P_{III}	
KS exchange	13.1	10.2	3.3	2.2	3.0	0.22
Slater exchange	11.0	8.5	2.2	1.7	2.5	0.30
Experimental	13.0	10.4	3.2	3.4	2.8	

The structure of bands 3 and 4 of ZrB_2 has a relative resemblance to the bands 3 and 4 derived from the $4d$ state in Zr band structure[19] except for a part along the ΓA line to which the boron planar layer affects. The band 1 of ZrB_2 behaves like the band 1 from the $5s$ state in the Zr band structure. Thus the band structure of ZrB_2 is thought to be determined by the sp^2 hybrid state and the p_z state of boron and the d and s states of zirconium. These results imply a possibility to explain the bonding nature of ZrB_2 by a combination of the graphite model of the boron network and the hcp-metal bonding model of zirconium.

The ratio of integrated intensities of peaks P_I, P_{II}, and P_{III} is approximately 1:1:3 in the calculated DOS, which indicates that the numbers of 2, 2, and 6 electrons contribute to these peaks,

respectively. The number of 6 electrons for peak P_{III} is nearly equal to 5.5 of the assumed d electrons estimated by Dempsey[4] for ZrB_2. This fact, however, would not necessarily mean a charge transfer from boron to zirconium, because peak P_{III} consists of hybrid states of the Zr $4d$ and the B $2p$ or p_z states. The direction of charge transfer between boron and zirconium cannot be determined in the present study, but probably charge transfer is unlikely or impossible to ZrB_2.

ACKNOWLEDGMENTS

[1]W. N. Lipscomb and D. J. Britton, J. Chem. Phys. 33, 275 (1960).

[2]A. H. Silver and P. J. Bray, J. Chem. Phys. 32, 288 (1960).

[3]Y. M. Garyachev, B. A. Kovenskaya, and G. V. Samsonov, Izv. Vyssh. Uchben. Zaved. Fiz. No. 8, 86 (1974).

[4]E. Dempsey, Philos. Mag. 8, 285 (1963).

[5]Y. S. Tyan, L. E. Toth, and Y. A. Chang, J. Phys. Chem. Solids 30, 785 (1969).

[6]H. J. Jeretschke and R. Steinitz, J. Phys. Chem. Solids 4, 118 (1958).

[7]R. Kiessling, Acta. Chem. Scand. 4, 209 (1950).

[8]A. J. McAlister, J. R. Cuthill, M. L. Williams, and R. C. Dobbyn, in Proceedings of the International Symposium on X-ray Spectra and Electronic Structure of Matter, Munich, 1972 [U.S. Govt. Rep. Announce. No. 74(13)] (U.S. GPO, Washington, D. C., 1974), Vol. 184, p. 23.

[9]S. H. Liu, L. Kopp, W. B. England, and H. W. Myron, Phys. Rev. B 11, 3463 (1975).

[10]P. G. Rerkins and A. V. J. Seeney, J. Less-Common Met. 47, 165 (1976).

[11]H. Ihara, Y. Kumashiro, and A. Itoh, Phys. Rev. B 12, 5465 (1975).

[12]H. Ihara, M. Hirabayashi, and H. Nakagawa, Phys. Rev. B 14, 1707 (1976).

[13]R. C. Linton, Thin Solid Film 20, 17 (1974).

[14]D. W. Fisher and W. L. Baun, J. Appl. Phys. 39, 4757 (1968).

[15]L. Ramqvist, B. Ekstig, E. Köllne, E. Noreland, and R. Manne, J. Phys. Chem. Solids 30, 1849 (1969).

[16]M. Hirabayashi and H. Nakagawa, in Proceedings of the 4th International Conference on Vacuum Metallurgy Tokyo, 1974 (unpublished), p. 267.

[17]W. Kohn and L. J. Sham, Phys. Rev. 140, A1133 (1965).

[18]P. O. Löwdin, Adv. Phys. 5, 1 (1956).

[19]F. Herman and S. Skillman, Atomic Structure Calculations (Prentice-Hall, Englewood Cliffs, N.J., 1963).

[20]T. L. Loucks, Augmented Plane Wave Method (Benjamin, New York, 1967).

[21]R. F. Willis, B. Fitton, and G. S. Painter, Phys. Rev. B 9, 1926 (1974).

[22]F. R. McFeely, S. P. Kowalczyk, L. Ley, R. G. Cavaell, R. A. Pollak, and D. A. Shirley, Phys. Rev. B 9, 5268 (1974).

[23]O. Jepsen, O. K. Anderson, and A. R. Mackintosh, Phys. Rev. B 12, 3084 (1975); T. L. Loucks, Phys. Rev. 159, 544 (1967).